PROGRESS REPORT

An Emerging Pore-Making Strategy: Confined Swelling-Induced Pore Generation in Block Copolymer Materials

Yong Wang and Fengbin Li*

Block copolymers (BCPs) composed of two or more thermodynamically incompatible homopolymers self-assemble into periodic microdomains. Exposing self-assembled BCPs with solvents selective to one block causes a swelling of the domains composed of this block. Strong swelling in the confinement imposed by the matrix of the other glassy block leads to well-defined porous structures via morphology reconstruction. This confined swelling-induced pore-making process has emerged recently as a new strategy to produce porous materials due to synergic advantages that include extreme simplicity, high pore regularity, involvement of no chemical reactions, no weight loss, reversibility of the pore forming process, etc. The mechanism, kinetics, morphology, and governing parameters of the confined swelling-induced pore-making process in BCP thin films are discussed, and the main applications of nanoporous thin films in the fields of template synthesis, surface patterning, and guidance for the areal arrangements of nanomaterials and biomolecules are summarized. Recent, promising results of extending this mechanism to produce BCP nanofibers or nanotubes and bulk materials with well-defined porosity, which makes this strategy also attractive to researchers outside the nanocommunity, are also presented.

1. Introduction

Pore size and distribution, the porosity and surface chemistry of pore walls, and pore structure determine the performance of porous materials in their applications, which include absorbents, separation filters, gas storage media, catalyst supports, templates for materials synthesis, and scaffolds for tissue engineering.[1,2] Numerous strategies have been developed to improve the pore properties, and nanotechnology and self-assembly play significant roles in pushing pores to ever-smaller dimensions, narrowing pore size distributions, and fabricating well-defined pore architectures.[3,4] Similar to the classification of nanomaterial preparation methods, the routes to making pores, including nanosized ones, can generally be divided into two groups: bottom-up and top-down. The self-assembly of colloidal crystals is a typical example of the bottom-up method, in which the porosity is defined by the gaps between the spherical colloids. Pores generated by this method are featured for their connectivity, that is, the pores form a continuous phase and are uniformly distributed throughout the material matrix. Pore size and size distribution are determined by the size and distribution of the self-assembled building blocks.[5] In the top-down process, some parts or components in a solid substrate are selectively removed, leaving pores in the substrate. The microfabrication of chips to create holes, channels, etc. can be regarded as being representative of this method. The top-down method is superior in its versatility of pore structures and ease of tuning the pore dimensions.[6] In addition, a templating method to prepare porous materials in which a template already carrying pores is filled with a precursor followed by template removal to give secondary porosity is also considered to be a top-down method, although it starts with porous templates and requires an additional step of pore filling compared to a typical top-down process.[7] In some cases, both bottom-up and top-down strategies are involved to build hierarchical, multiple scale pore systems.[8,9] However, in both methods, there is a constant demand to make pores using a simple process that is highly efficient and low cost.

Block copolymers (BCPs) have recently been extensively exploited for the preparation of porous materials with well-defined nanopores in various ways and BCPs perform different functions in the pore-making process. BCPs are composed of two or more chemically distinct homopolymer chains covalently linked together. Because of the thermodynamic incompatibility of the homopolymer chains, BCPs tend to phase-separate like polymer blends. However, due to the covalent bonding between blocks, their phase separation can only occur on the microscale, which is therefore called "microphase separation", resulting in separated domains typically on the scale of 10–100 nm. Furthermore, since BCPs are usually synthesized by controlled living polymerization, their molecular weight distribution can be well controlled in a very narrow range, which dictates the monodispersive size distribution of the phase-separated domains. By changing volume fractions of the constituent blocks, a series of delicate and well-ordered phase-separated morphologies, including spheres, cylinders, gyroids, and lamellae, appears in the bulk state of the BCPs.[10–13] When dissolved in a solvent that is selectively preferential to one block, the BCPs

Prof. Y. Wang, F.-B. Li
State Key Laboratory of Materials-Oriented Chemical Engineering and College of Chemistry and Chemical Engineering
Nanjing University of Technology
Nanjing, Jiangsu, 210009, P. R. China
E-mail: yongwang@njut.edu.cn

DOI: 10.1002/adma.201004022

self-assemble to form micelles, and while in thin film or other low dimension configurations, microphase separation also takes place and produces well-defined morphologies that are sometimes unavailable in their bulk counterparts.[14] It is well-documented that BCPs self-assembled in different forms, such as as micelles and thin films, play an active role in the preparation of a huge library of nanostructures, including porous materials with well-defined pore architectures[15–17] The best known strategy in this regard is to prepare nanoporous metal oxides, e.g., silica, titania, etc., using amphiphilic block copolymers, such as poly(ethyl oxide)-*b*-poly(propyl oxide)-*b*-poly(ethyl oxide) (PEO-*b*-PPO-*b*-PEO), as templates to direct the sol-gel process of inorganic precursors.[18,19] In this method, the BCPs form micelles in selective solvents and precursor molecules complex with BCP micelles, forming regular self-assembled structures. In the subsequent calcination or extraction step, the space preoccupied by the BCPs is converted to pores with the complete removal of the BCPs, leaving a nanoporous inorganic framework. The pore size of the generated porous materials is mainly determined by molecular weight and the block ratio of the BCPs used, and predominantly falls into the range of 1–10 nm. This BCP micelle templating method is generally limited to the preparation of nanoporous metal-oxide-, metal-, or carbon-based "hard materials" and there are few reports of the production of nanoporous polymer-based "soft matter" via this method.

On the other hand, BCP thin films or bulk materials can be transformed to polymer-based porous materials independently or with the aid of a small amount of additives. In this strategy, BCP is the single or predominant starting material and one BCP block or additive is selectively removed to form pores. The remaining blocks hold the integrity and mechanical stability of the final porous polymer materials. One straightforward approach begins with pure BCPs in which one block is selectively etched away. However, the etching methods are polymer-specific and thus vary with the BCPs used. Very limited types of BCPs with labile blocks are eligible for this purpose: for instance, BCPs containing poly(methyl methacrylate) (PMMA),[20,21] polylactide,[22,23] and polymers with double bonds, e.g., polybutadiene or polyisoprene,[24,25] which can by etched away by short-wavelength UV light exposure, hydrolysis, and ozonolysis, respectively. An alternative way is to include additives (i.e., small molecules or even homopolymers with low molecular weights, which are also one of the constituent blocks of the BCP) into the BCPs.[26,27] The additives bind to one block of the BCPs via hydrogen bonding or coordination to form complexed BCPs, which behave similarly to free BCPs and produce well-defined phase-separated morphologies. In a case where homopolymers are the additive, they dissolve into the domains of the same block in the copolymer. The space preoccupied by the additives is converted to empty pores by extraction from the domain using a selective solvent, leading to porous polymeric materials with regular pores typically in the range of 10–30 nm.[28,29] Both methods mentioned here are elegant in pore size control and frequently used by many researchers. However, they suffer from tedious and time-consuming preparation protocols. In addition, in both methods, pores are generated by sacrificing one block or the additives, which results in mass loss. This mass loss may reduce the robustness of the porous materials produced and cause extensive washing and post-treatment efforts in the extraction step. Hillmyer and colleagues provided two excellent reviews on the topic of nanoporous materials derived from BCP precursors.[30,31] Readers are directed to these reviews and the references therein for details, while we focus on another strategy for making porous materials from BCPs. This strategy emerged very recently and has not been covered in previous reviews.

The new approach uses purely block copolymers and the pore-forming mechanism is based on a physical phenomenon that involves no chemical reaction. It is an extremely simple method: one needs only to immerse BCP materials, i.e., 1D nanofibers, 2D thin films, or 3D bulk materials, in a certain solvent for hours (sometimes less), then remove them, and evaporate the solvent to obtain the porous materials with ordered pore systems. The profile of the BCP materials remains unchanged. In this method, the confined swelling and subsequent drying of domains of the minor blocks confined in the continuous phase of the major blocks, which are still in a glassy state, is responsible for pore generation. Therefore, this method is called "confined swelling-induced pore generation". Here, after the introducing the current techniques for BCP-based porous materials mentioned above, we will describe in detail the confined swelling-induced pore generation in the 2D BCP thin films to which the concept was initially applied. The mechanism for pore formation, kinetic control of the pore-forming process, and the morphological features of the resulting porous structure will be discussed, followed by a summary of the applications of the resultant nanoporous thin films. The adoption of this method to BCP systems of 1D nanofibers and 3D bulk materials is described, followed by brief concluding remarks about this method.

Yong Wang earned his PhD in Chemistry from the Chinese Academy of Sciences in 2005. He worked briefly as a Research Scientist at Procter and Gamble and then worked as a Humboldt Research Fellow with Prof. Martin Steinhart and Prof. Ulrich Gösele at the Max Planck Institute of Microstructure Physics from 2006 to 2009. He is currently a Professor at the State Key Laboratory of Materials-Oriented Chemical Engineering, Nanjing University of Technology. His research interests include block copolymers and advanced deposition techniques for functional materials, with high-resolution separation membranes as the current focus.

2. Confined Swelling-Induced Pore Generation in 2D BCP Thin Films

The phenomenon of confined swelling-induced pore generation was first accidentally discovered in the systems of amphiphilic BCP micellar monolayers.[32] When dissolved in nonpolar solvents, amphiphilic BCPs form reverse micelles with nonpolar blocks extending in the solvent as coronas and with polar blocks collapsed in cores. When spin-coated or dip-coated, these micelles can be transferred to smooth planar substrates, leading to micellar monolayers. The solvent-swollen coronas of neighboring micelles touch and fuse in the solvent-evaporation procedure, resulting in a continuous thin film with the protruding micelle cores periodically embedded in the film. The first study on selective solvent-induced surface reconstruction on amphiphilic BCP micellar films was carried out on free-standing monolayers of polystyrene-*block*-poly(4-vinyl pyridine) (PS-*b*-P4VP) micelles by Sohn et al.[33] They observed a complete core –corona inversion in which the initial micelle-core-forming P4VP chains migrated to the surface and wrapped the condensed PS chains. The surface of the inverted film maintained its smoothness (although it was slightly rougher than the untreated surface) and no particular pattern could be found on it. However, in most cases, micellar monolayers were deposited on smooth substrates and were used for various applications together with their supporting substrates for easy handling. When exposing the supported micellar films to a polar solvent, the core –corona inversion will be considerably restricted because of the presence of the substrate on which the polymer chains will be tightly attached. Therefore, the selective solvent-induced surface reconstruction can only occur in the upward direction, forming surface cavities caused by the breaking of the coronas by expanding micelle cores, while the bottom base of the film remains undisturbed. This confined swelling-induced pore generation in 2D BCP micellar films was observed in various amphiphilic BCPs, among which polystyrene-*block*-polyacrylic acid (PS-*b*-PAA) and polystyrene-*block*-poly(*x*-vinyl pyridine) (PS-*b*-P*x*VP; $x = 2$ or 4) were most frequently used.[32,34–37]

2.1. Mechanism of Pore Formation Induced by Confined Swelling

The mechanism for the pore formation in the swelling and subsequent drying process is straightforward and is somewhat analogous to the swelling of rubbers, which commonly involves the elastic deformation of a crosslinked network structure by solvent uptake.[38] In the exposure of a solvent selective to the core-forming blocks, the solvent will penetrate through the thin corona, diffuse into the micelle cores, and be taken up by the cores. Because of the strong affinity between the solvent and the core blocks, the macromolecular chains of the cores will take on a stretched conformation, with significantly expanded volume, which is typically called "swelling".[39] However, since the cores are confined in glassy coronas, pressure is exerted on the nonswollen, corona-forming domains, which consequently undergo plastic deformation. When the pressure accumulated in the swelling process exceeds the tensile strength of the corona, the micelle corona ruptures via disentanglement of the corona chains, and the core chains overflow from the initial position of the core and are exposed to the solvent, directly shielding the energetically unfavorable contact between the solvent and the nonswollen components. With solvent evaporation in the drying process, the deformed structure of the nonswollen matrix is fixed and the swollen core-forming chains shrink and collapse on the matrix wall, forming pores at positions corresponding to the initial micelle cores.

In the most extensively studied case of the swelling of PS-*b*-P2VP by ethanol, PS chains are still in the glassy state when exposed to ethanol at room temperature. Ethanol diffuses into the PS coronas very fast since the PS corona is very thin, on the order of several nanometers. For example, for a PS-*b*-P2VP polymer with a PS molecular weight of 102 000 and a P2VP molecular weight of 97 000, the average diameter of the dry micelles prepared from *o*-xylene is ≈53 nm and the thickness of the PS corona can be estimated to be ≈5 nm.[40] With the continuous diffusion of ethanol molecules into micelle cores, P2VP keeps swelling, driving cores to expand. However, since P2VP cores are confined in the glassy PS corona, the expansion of the P2VP cores is prohibited. Protruding of micelles in the upward direction may happen at the very initial stage of swelling since the micelle is restricted by the hard substrate that cannot be deformed downward and by neighboring micelles in the direction parallel to the surface of the substrate. However, this initial protrusion will quickly develop into a rupture of the PS corona. This is because the glassy, rigid, and ultrathin PS micelle corona cannot release the tensile force accumulated from the continuous swelling by an adequate elastic deformation. The rupture is most likely to occur in the thinnest region of the micelles in the as-coated PS-*b*-P2VP film since these points are the weakest.

During the confined swelling of the minor phases (micelle cores) distributed in the glassy film matrix, the cores undergo a drastic morphological reconstruction, forming pores, accompanied by a slight and local plastic deformation of the glassy nonswollen component adjacent to the micelle cores. Meanwhile, the thin film configuration of the BCP system remains mostly undisturbed because the nonswollen matrix is still in the glassy state when exposed to the solvent. This fact implies that the patterning and ordering of the pores in the surface of the reconstructed film are predetermined by the periodicity of the pristine BCP micellar film, which makes it possible to fabricate near-perfectly ordered porous surfaces by swelling micellar films with ordering achieved by optimized solvent annealing.[41] **Figure 1** shows an example of the near-perfect ordering of a solvent-annealed micellar film and the corresponding porous film obtained by the confined swelling.[41a]

2.2. Kinetic Control of the Pore-Forming Process

In the course of swelling-induced pore generation, changes in the Gibbs free energy, *G*, arise due to contributions from the mixing of the swelling solvent and swelling blocks, the chain stretching, and the interfacial energy of the nonswollen domains. Therefore, enthalpic interactions between the swelling solvent and swelling blocks determine the degree of swelling at a given temperature and, consequently, influence the ultimate

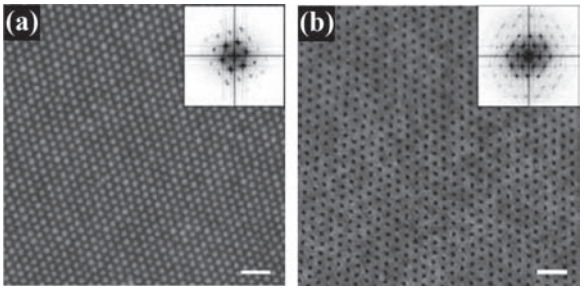

Figure 1. Scanning force microscopy surface images of the PS-*b*-P4VP micellar films before (a) and after (b) the morphology reconstruction induced by ethanol immersion for 30 min, showing the near-perfectly hexagonally patterned micelle protrusions and pores on the BCP films, respectively. The ordering of the as-cast film was improved by solvent annealing in toluene. Strong multiple peaks of the Fourier transforms in the insets suggest the long-range ordering of both the micelle protrusions and the pores. Scale bars correspond to 200 nm. Adapted with permission.[41a] Copyright 2010, The Royal Society of Chemistry.

endpoint of the swelling-induced morphology reconstruction. To a weaker extent than the affinity between the solvent and the swelling blocks, the affinity between the swelling solvent and the nonswollen component also influences the pore generation process in the steps of the diffusion of the solvent through the micellar corona, and the plastic deformation of the glassy matrix in which the swelling solvent functions as a plasticizer improving chain mobility.[41b,c] Miller and co-workers treated thin films of PS-*b*-PAA micellar monolayers with alkyl alcohols of varying chain lengths and observed pore formation in films treated with alcohols with ≤3 carbon atoms, while no pore was developed in cases using higher alcohols including *n*-butanol and *n*-octanol. Lower alcohols, e.g., methanol, ethanol, and propanol, have stronger polarity and greater affinity to PAA blocks, allowing for the intensified swelling of the PAA cores and rupture of the PS coronas.[42] Moreover, enthalpic interactions between the swelling solvents and the swelling blocks not only control the thermodynamic but also the kinetics of the pore formation process. Swelling solvents with different affinities to swelling blocks take different lengths of time to complete the pore-forming process. The pore formation can be terminated simply by withdrawing the films from the solvent, thus freezing intermediate opening pore morphologies with various pore sizes and surface topographies. **Figure 2** shows four intermediate porous morphologies obtained by incubating PS-*b*-P2VP micellar films in water (pH = 8) for different periods of time ranging from 30 s to 18 h.[40] In addition, it was found that in the same BCP system the pore openness of the BCP film treated in water (pH = 8) for 18 h was similar to that of the BCP film treated in ethanol for only 30 s, mainly because ethanol has a stronger interaction to P2VP chains than water (pH = 8), while the difference between the affinity of ethanol and water to PS chains into which the swelling solvents penetrate plays a minor role. Since the micelle cores forming blocks are often weak polyelectrolytes, for instance, P2VP, P4VP, and PAA, some solution properties, such as pH values and ionic strength, greatly influence the kinetics of the pore-forming process, facilitating more controls in finely tuning the sizes and morphologies of the resultant pores. In the micellar films of PS-*b*-PAA, it was

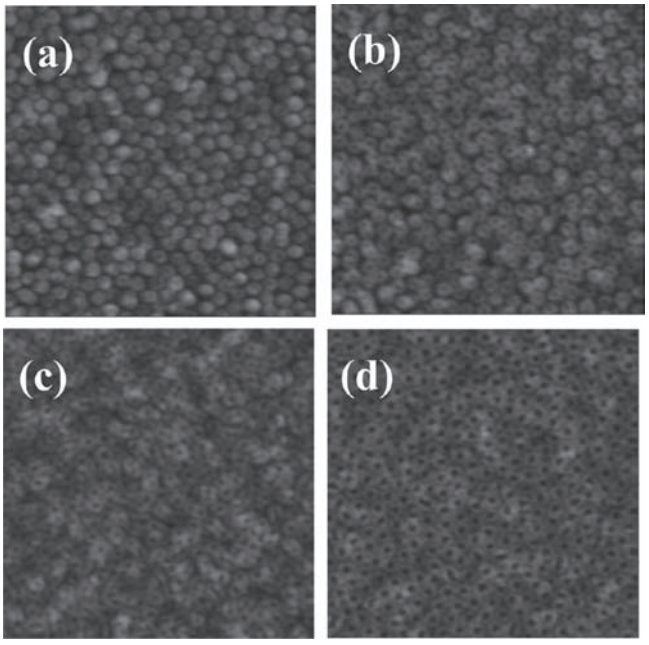

Figure 2. Atomic force microscopy images of PS-*b*-P2VP micellar films immersed in water with pH = 8 for different periods of time: a) 30 s, b) 3 min, c) 30 min, and d) 18 h, demonstrating the slow pore-opening process of the BCP film in slightly basic aqueous ambient and the possibility to delicately tune the pore morphology by changing the swelling conditions, for example, the swelling time. The scan size of these AFM images is 1 μm × 1 μm. Reproduced with permission.[40] Copyright 2010, American Chemical Society.

demonstrated that an increase in the pH value of the water in which BCP films were incubated led to faster pore forming and larger pore sizes, while it exerted a completely opposite effect in the case of PS-*b*-P2VP.[40]

2.3. Morphology Tuning of the Pores

If the intermicelle distance is larger than the diameter of the micelle,[43] a swelling-induced morphology reconstruction of the individual micelles takes place, and each micelle transforms into a ring-like opening structure since there is no chance for the swelling chains that overflow from neighboring micelle cores to meet and fuse.[44] On the other hand, the structural parameters of the as-cast BCP micellar films are strongly dependent on the molecular weights of the constituent blocks, and thus, pore size, interpore distance, and the areal pore density of the cavitated films are closely associated with the molecular weight of the blocks.[45] Moreover, since the molecular weight of each constituent block has a great influence on the aggregated number, core size, and corona thickness of the micelles prepared under certain conditions, micellar films prepared from BCPs composed of the same blocks but different molecular weights vary in the size of the swellable cores as well as the thickness of the nonswollen corona. Therefore, under the same swelling conditions, they exhibit different pore-forming kinetics and various equilibrium porous morphologies, and in cases of highly asymmetric BCPs with much longer

nonswollen blocks, the swelling-induced pore generation may not occur at all because the moderate swelling tendency of the cores cannot break through the tight confinement of the thick glassy coronas.[42] Lastly, since *G* is commonly a function of temperature, swelling temperature also plays a significant role in the pore-generation process. However, in most cases of BCP thin films, pore generation takes place easily at room temperature because the capping nonswollen corona is extremely thin, typically less than 10 nm, and the moderate swelling of the cores can rupture it, forming pores.[40] The temperature effect becomes apparent in the case of very tightly confined domains in BCP 1D nanofibers/tubes and 3D bulk materials that can be swollen and this will be revisited later.

Although the 2D BCP thin-film systems discussed above are predominantly micellar monolayers in which the cores that can be swollen are completely entrapped by nonswollen coronas, it should be noted that this swelling-induced pore generation also occurs in other configurations of BCP thin films in which the domains oriented perpendicular to the substrate are distributed as the minor phase in the nonswollen matrix.[46] The difference between the two thin-film systems is that the swellable domains in the latter case are only partially surrounded by the nonswollen components, leaving a free upper side, which may facilitate solvent uptake and the overflow of the swelling blocks in the solvent exposure.

In the confined swelling-induced morphology reconstruction, after the solvent evaporation in the drying stage, the core-forming block chains overflow from the core, migrate, and are deposited on the surface, covering the nonswollen blocks either partially or completely, depending on the swelling degree of the chains. This migration of chains that can be swollen onto the film surface leads to a noticeable, typically ≈10% increase in film thickness[47,48] and a change in surface properties, for instance, hydrophilicity, which was confirmed in various BCPs by means of measuring water contact angle and X-ray photoelectron spectroscopy (XPS) analysis.[40,47,49]

As mentioned previously, it may take hours or longer to complete the confined swelling-induced morphology reconstruction in the case where the swelling solvent only shows a moderate affinity to the swelling blocks, for instance, when water (pH = 8) swells P2VP domains in PS-*b*-P2VP micellar films. The termination of this slow swelling process intermediately leads to an inadequate release of the swellable blocks from the cores, and the residual swellable blocks still remain in the bottom of the initial micelle cores. As a result, intermediate open morphologies of shallow dimples appear instead of deep pores, with depths close to the film thickness. However, even in the case of complete surface reconstruction, there is still an argument about whether the resultant pores are through-holes that span the entire thickness of the film or the bottom side of the pores is blocked by a thin polymer layer in contact with the substrate. Li et al. accessed the bottom surface (the side in contact with the substrate after the film-cast process) of a PS-*b*-P2VP micellar film by floating the reconstructed film (induced by acetic acid incubation) in an aqueous solution and transferring it to other substrates with the bottom surface up; they found that the bottom side was skin-free and had a porous morphology similar to that of the upper side observed by atomic force microscopy.[50] However, there is a strong possibility that the porous structure on the bottom surface was developed in the film floating and transfer steps rather than during the initial acetic acid immersion. Aqueous solutions were used extensively during film floating and transferring, and these may induce a morphology reconstruction to the exposed bottom surface, since it was previously demonstrated that water, even in the a weak basic or neutral state, is capable of triggering the rupture of PS coronas to form pores by the swelling of P2VP blocks.[40] On the other hand, it is reasonable to assume that the rupture of micelle coronas cannot take place from the bottom side, which contacts the substrate, because of the tight confinement of the rigid substrate that can not be deformed, and the accumulated pressure from swelling can only be released from the weakest points, i.e., the cap of the micelle coronas. Even for BCP films prepared from neutral solvents in which no micelle forms and the swellable domains are directly exposed to the air and substrate sides without the cushion of the nonswollen blocks in micellar films, the presence of a thin polymer layer underneath the pores produced by swelling in PS-*b*-P4VP films was demonstrated.[51] In another case, Xu et al. employed grazing incidence small angle X-ray scattering (GISAXS) and X-ray reflectivity techniques to compare the film thickness and pore depth of PS-*b*-PMMA films in which the PMMA domains were selectively swollen by acetic acid and transformed into channel-like pores, demonstrating that the pores traversed throughout the entire film thickness. However, they found during the course of acetic acid treatment, some PMMA chains from the block copolymer migrated to the underlying PS/PMMA random copolymer brush layer (this random copolymer brush was grafted on to the substrate to balance the interfacial energy for the purpose of inducing the perpendicular orientation of PMMA domains), increasing the brush layer thickness by ≈1 nm.[52] Due to to the ultrathin nature of the polymer layer that cushions the pores, typically only a few nanometers, electron tunneling takes place[51] and makes it possible to carry out electrochemical reactions across the ultrathin polymer layer under the porous film templates supported on conductive substrates to grow various types of nanomaterials.[50]

2.4. Conditions for Pore Formation

A variety of BCPs, including PS-*b*-P2VP, PS-*b*-P4VP, PS-*b*-PAA, and polystyrene-*block*-polyethylene oxide (PS-*b*-PEO) in the strong aggregation limit and polystyrene-*b*-poly(methyl methacrylate) (PS-*b*-PMMA)[47,52–54] in the weak aggregation limit, were reported to undergo a swelling-induced pore-forming morphology reconstruction under appropriate swelling conditions. There are a few general rules governing the occurrence of this type of morphology reconstruction.[55] First, the nonswollen blocks should be in the glassy state at the swelling temperature to keep the overall structure of the BCP material stable during the swelling. Second, the swellable domains need to be the dispersive phase and need to be distributed separately in the matrix of the nonswollen components. This requirement ensures that swelling takes place selectively in scattering positions confined by the glassy, nonswollen components to prevent collapse of the overall structure. It should be noted that this does not exclude the possibility of micellar films of asymmetric BCPs

Table 1. A brief summary of the material requirements, swelling conditions, and attainable pore morphologies of the confined swelling-induced pore-making method.

Items	Specific requirements or range of values
Types of BCPs	Mainly amphiphilic BCPs, e.g., PS-*b*,P2VP [Ref. 40, 44, 55, 65, 66, 75, 76, 82, etc.], PS-*b*-P4VP [Ref. 33, 40, 48, 67–70, etc.], PS-*b*-PAA [35, 36, 41, 45, etc.], PS-*b*-PEO [Ref. 74], and PS-*b*-PMMA [Ref. 47, 52–54, etc.].
Volume fractions of the nonswelling blocks	>50% [Ref. 33, 44, 54, 64, etc.], and larger, within a range of 70–90% [Ref. 40, 55, 75, 76, 82, etc.], with the exception of the micellar BCP films where the volume fraction of the nonswelling block can be <50% [Ref. 46].
Glass transition temprature (T_g) of the nonswelling blocks	Above room temperature; polystyrene-based BCPs are predominantly used and PS has a T_g of ≈100 °C [Ref. 40, 55, 75, 76, 82, etc.].
Difference in solubility parameters of constituent blocks	The larger the better, but boundary conditions not yet determined.
Swelling solvents	Should be good solvent for the minor component and nonsolvent for the major component. For the most frequently used PS-*b*-PxVP BCPs, water [Ref. 40, 44, 65, 66, 75, etc.], ethanol [Ref. 40, 62, 64, 67–70, 76, etc.], acetic acid [Ref. 50, 75], glycerol [Ref. 71], etc. were used as swelling solvents.
Swelling temperature	Lower than T_g of the major component: room temperature [Ref. 33, 35, 41, 45, 48, 62, 64, 67–70, etc.] and 60 °C [Ref. 55, 75, 76] are typically used for PS-based BCPs.
Swelling time	From instantaneous to hours, depending on the thickness of the BCP materials and affinity of swelling solvents to both blocks: seconds [Ref. 33, 41, 45, 48, 62, 64, 67–70, etc.], minutes to hours [Ref. 55, 75, 76, etc.].
Attainable pore geometry	Spherical [Ref. 55], cylindrial [Ref. 48, 62, 64, 67–70, etc.], and bicontinuous [Ref. 55, 76] pores according to the equilibrated morphologies of the starting BCPs.
Attainable pore diameter	Typically ≈10 to 100 nm, depending on BCP molecular weight and volume fraction of the minor component [Ref. 48, 55, 62, 64, 67–70, 76, etc.].

with longer swellable blocks undergoing surface reconstruction because such BCPs are also capable of forming crew-cut micelles with a large core of swellable chains and a very thin corona of nonswollen blocks.[14,46] Upon casting, these micelles form films via the fusion of the neighboring micelle coronas with the micelles cores still separately embedded. Third, there should be a strong difference in the selectivity of the swelling solvent to the two blocks. A large difference in affinity allows adequate swelling to occur highly selectively in the swellable domains while the matrix is undisturbed. Based on the above considerations, it is assumed that many more combinations of BCPs and swelling solvents can be explored to induce the pore-forming morphology reconstruction. In an interesting example, Yokoyama and co-workers reported that solid films of fluorinated BCPs, such as polystyrene-*block*-poly(perfluorooctylethyl methacrylate), could be turned into nanoporous films by treating them in compressed carbon dioxide through the same confined swelling-induced pore-formation mechanism. In their work, the domains of the fluorinated blocks, which had either spherical or lamellar morphology, were saturated and swollen with carbon dioxide, thus expanding the volume, and pores formed after the release of carbon dioxide at a lower temperature to freeze the PS matrix.[56] Carbon dioxide worked as a swelling solvent with a pressure-controlled, tunable affinity for the fluorinated blocks.[57] The affinity of carbon dioxide to fluorinated blocks is much weaker than that of liquid solvents to the corresponding swellable blocks, for instance, the affinity of ethanol to P2VP. As a result, the domains of the fluorinated blocks were swollen to a limited degree, which was insufficient to trigger the rupture of the PS corona, even at an elevated temperature of 60 °C. Therefore, the obtained pores were embedded in the film with a dense skin and could be exposed to the surface only after etching away the surface skin. In addition, the CO_2-induced pore generation was observed again in films of PS-*b*-PMMA.[58] Compressed CO_2 was also successfully used as a plasticizer to enhance the methanol swelling of P2VP domains and to accelerate the transport of methanol in PS-*b*-P2VP thick films.[59]

Based on the discussion in this section, the material requirements, swelling conditions, and attainable pore morphologies produced using this method of confined swelling-induced pore generation are briefly summarized in **Table 1**. This may serve as a preliminary guide for the development of porous materials using this method, even though the contents of this table are still rough and far from complete due to the limited available data.

3. Applications of the Confined Swelling-Induced Nanoporous Films

The applications of the nanoporous films prepared using the method of confined swelling-induced pore generation are based on the collective superior properties of the nanoporous films, which include small pore size (typically less than 50 nm), narrow pore size distribution, the achievable long-range ordering of the pore arrangement, the strong contrast in the structure and chemical properties of the open and the covered areas, and easy and reversible switching between the open and closed pore state. The nanoporous thin films are mainly used in three different applications: template synthesis of regular arrays of nanomaterials, e.g., nanodots and nanorods; surface patterning on various substrates; and guidance of areal arrangements of nanomaterials and biomolecules. These applications originate either from the structural variety or chemical heterogeneity of the open pores and solid surfaces, or in some cases both.

3.1. Template Synthesis

On selective solvent-treated BCP thin films, well-defined nanopores are periodically distributed in the film matrix, resulting

in a strong contrast in structural variety between the empty pores and the solid polymer matrix. It is straightforward to use these pores as templates to synthesize nanomaterials with corresponding structural features. Li et al. treated PS-*b*-P2VP micellar films supported on gold substrates with acetic acid immersion, producing nanoporous films and electrodeposited polyaniline (PANI) onto the template films. They found that during the initial stage of the electropolymerization the nucleation sites formed only at the position of the pores, and PANI continued to grow from the nuclei because only the porous regions were exposed to the electrodeposition solutions, which defined the places where the reaction could take place. After removing the BCP template, they obtained PANI nanorods, the diameter of which was identical to that of the template pores independent of the experimental conditions. The diameter of the PANI nanorods could be tuned by controlling the pore size. When the height of the PANI nanorods exceeded the depth of the template pores, the growth rate of PANI increased and the templating effect of the pores faded away, leading to porous films composed of intertwined PANI nanofibers.[50]

In contrast to other templates with cylindrical nanopores, such as anodized aluminum oxides[60] and track-etched membranes,[61] the aspect ratio of the template pores in the nanoporous BCP thin films is considerably low, typically less than 3. This low aspect ratio limits the length of the templated 1D nanostructures or easily results in overgrowth outside of the template pores. However, in some cases, this overgrowth is desirable for the preparation of hierarchical nanomaterials with a templated regular structure on the bottom and an overgrown impinging structure on the top. The hierarchical structure may display interesting properties that are inaccessible using regular structures obtained by the single template effect. For instance, Wang and co-workers exposed acetic-acid-treated PS-*b*-P2VP micellar films supported on silicon substrates to an aqueous plating solution of $NaAuCl_4$ and HF. The solution contacted the exposed silicon substrate via the pores, and the galvanic displacement reaction between $[AuCl_4]^-$ and the silicon occurred with the aid of HF, etching away the SiO_2 barrier layer in the porous regions. The galvanic reaction resulted in the deposition of gold in the pores and the partial dissolution of underlying silicon substrates. They obtained gold nanostructures with different morphologies by changing the plating time. With a short plating time, e.g., 15 s, the galvanic displacement reaction only took place inside the template pores and resulted in arrays of gold nanopillars supported on a continuous gold film. The short gold pillars were replicas of the nanoporous BCP templates. After the template pores were fully filled with the deposited gold, continuous reaction led to an overgrowth of gold, which formed mushroom-like caps on tops of the gold pillars. Longer plating caused the caps to merge into a thick gold film on top of the BCP template (**Figure 3**). The gold pillars with mushroom-like caps, obtained at a moderate plating times, showed significantly enhanced Raman scattering performance compared to other gold nanostructures prepared at shorter or longer plating times. This enhanced Raman effect is a consequence of the high spatial density of the hot spots that are present in narrow gaps between the sharp edges of the impinging caps, which facilitates the formation of a strong field enhancement because of the large curvature and interparticle coupling.[62] In addition, Qiao and co-workers confined the etching of silicon by HF selectively in the open area of PS-*b*-P4VP micellar films and obtained arrays of nanosized holes on the surface of the silicon substrates. In this research, BCP micellar-film-coated silicon was immersed in a dilute HF solution and HF served two purposes. First, the initial uptake of HF facilitated the opening of P4VP cores in an aqueous environment by protonizing the pyridyl groups. Second, HF worked as an etchant to react with the silicon just below the core positions, where the thickness was much thinner due to the escape of P4VP chains. As a result, there was an enhanced HF diffusion approaching the silicon substrates. Again, the periodicity of the surface holes mirrored that of the parent BCP templates. Fine control of the shapes, sizes, average spacings, and surface chemistries of the holes was demonstrated by changing the molecular weight and block ratio of the BCPs, the orientation of silicon substrates, and other etching parameters.[63] The success of the reconstructed BCP film-confined chemical reactions implies that even though it is possible that a thin polymer layer exists at the bottom of the pores in the reconstructed BCP films, as discussed in Section 2.3, this layer is extremely thin and can be regarded as "diffusion-transparent". Reactants can penetrate it very quickly and react with the underlying substrate. Reactions that are appropriate to be confined predominantly at the position of pores need to be anisotropic, that is, the reaction rate in the direction perpendicular to the substrate surface should be much higher than that in the direction parallel to the substrate surface. Otherwise, horizontal reaction fronts in neighboring pores, which typically have a spacing of several tens of nanometers, will meet within a very short period of time. This early coalescence of reaction fronts will lead to very shallow holes on the surface, or even worse, the failure of the areal selectivity of the reaction and, consequently, the loss of the periodicity of the nanostructures obtained.

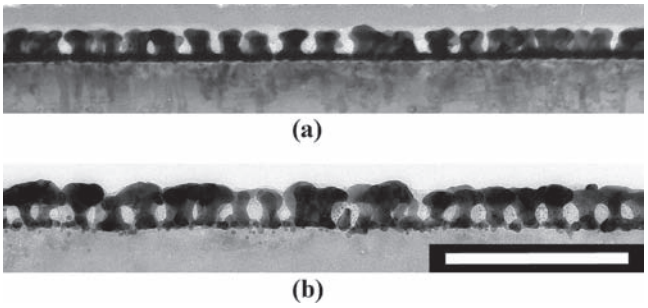

Figure 3. Cross-sectional transmission electron microscopy images of thin slices of silicon with different pillar-like gold nanostructures obtained by a galvanic displacement reaction between $NaAuCl_4$ and silicon templated by reconstructed PS-*b*-P2VP films in the presence of HF: a) the structure obtained at an earlier stage (15 s) before the occurrence of the overgrowth of gold outside the BCP template pores and b) the structure obtained at a later stage (30 s) when the overgrowth of gold had already taken place. Panels (a) and (b) have the same magnification. The scale bar in (b) is 200 nm. Reproduced with permission.[62] Copyright 2009, American Chemical Society.

In addition to confining chemical reactions to the porous region of the reconstructed BCP thin films and obtaining nanostructures that copy the structural features of the pores,

Wang et al.[64] converted the reconstructed PS-*b*-P2VP micellar films to ultrathin carbon films with corresponding surface pores. In this case there was a large shrinkage in the film thickness and pore size. However, the ordering and periodicity were preserved due to the strong confinement of the pristine BCP films on the substrates. The BCP films served as both templates and carbon precursors. Through stabilization by UV-exposure-induced crosslinking and subsequent direct carbonization steps, both blocks in the BCP films were transformed to carbonaceous material, allowing for a faithful structural transfer in the harsh carbonization process. Significantly, patterned films of polymeric materials, which are typically vulnerable and non-conductive, were converted into robust, chemical-resistant, and conductive carbonaceous counterparts with similar structural features, thus magnifying the applications of patterned thin films in more diverse circumstances.

On the other hand, the chemical heterogeneity of the constituent blocks of the BCP materials also plays a significant role. The blocks are thermodynamically incompatible and have a pronounced difference in physical and/or chemical properties, allowing the formation of micelles in selective solvents and selective solvent-induced morphology reconstruction in BCP thin films. For the amphiphilic BCPs, e.g., PS-*b*-PVP, PS-*b*-PAA, the major component (usually PS) is relatively chemically inert, holding the framework and providing mechanical stability to BCP materials. In contrast, the minor component, e.g., PVP or PAA, is a polyelectrolyte that has a strong ability to interact with other species through coordination, electrostatic interactions, or even covalent bonding. Metal ions can be incorporated into micelle cores through coordination and/or electrostatic interaction, allowing for the subsequent production of metallic structures with periodicities identical to those of the micelle patterns. Since the as-cast micellar film is covered by a hydrophobic layer, which prevents the efficient contact of the metal ions in the solution and core-forming polyelectrolyte chains, the metal incorporation process decelerates significantly. Therefore, it is very helpful, or in some cases necessary, to open the micelle cores before or during the metal ion incorporation process through the confined swelling mechanism to facilitate the binding of the metal ions of the polar chains. Chai and co-workers exposed PS-*b*-P2VP micellar films to a dilute acidic solution of metal salts to incorporate negatively charged metal ions into positively charged protonated P2VP blocks through electrostatic attraction. The metal-ion-incorporated BCP films were then subjected to a short oxygen plasma treatment to remove the polymer templates and convert the metal ions into elementary metals, leading to continuous metallic nanowires. It was found that the acidic nature of the solution was necessary for the enhancement of the P2VP swelling to break the PS barrier and facilitate the metal loading process. The versatility of this method was demonstrated through tuning of the nanowire composition, dimension, spacing, and orientation by manipulation of the solution concentration, deposition time, molecular weight of the BCPs, and other experimental parameters.[65,66] In addition to facilitating metal incorporation, the varied of pore openings caused by different degrees of swelling of the BCP micellar films offer the possibility to fabricate gold nanostructures with correspondingly different morphologies. For instance, Wang et al. observed the formation of ringlike openings in sparsely arranged PS-*b*-P2VP micellar films that were briefly treated in a dilute HCl solution (0.9 wt%). They demonstrated that the ringlike structure could be coined to produce arrays of gold nanorings with the periodicity of the pristine micelles by immersing the same PS-*b*-P2VP micellar film in a dilute acidic solution of $HAuCl_4$ followed by exposure to an oxygen plasma. Once again, they confirmed the importance of the acidic nature of the metal salt solution, which protonized P2VP and led to pore formation due to strong and fast swelling. On the other hand, in a non-acidic ethanolic solution, the metal-loaded P2VP cores were insufficiently swollen and core opening could not take place. This led to the production of solid gold nanoparticles instead of nanorings after plasma treatment.[44]

3.2. Surface Patterning

Due to the uniform pore size and ordering, as well as the ultrathin thickness of the swelling-induced nanoporous BCP films, the pores were extensively exploited as etching masks for surface patterning on various substrates based on their lateral structure variety. In these applications, plasma etching was directed to the exposed areas on the substrate surface through the open pores, and the polymer matrix acted as a sacrificial layer shielding the underlying substrate from attack by the plasma before it was consumed. Krishnamoothy and co-workers immersed PS-*b*-P2VP micellar films spin-cast on silicon substrates in methanol to develop nanoporous structures. They then subjected the substrate to SiF_6 plasma to etch the exposed silicon surface and then removed the remaining polymer masks using oxygen plasma etching. They obtained shallow surface holes with a cup-shaped geometry on silicon substrates, which maintained the ordering and periodicity of the BCP mask. The dimensions and periodicity of the surface holes could be tuned by using BCPs with different molecular weights.[49] Similarly, Kim and co-workers etched nanoporous PS-*b*-P4VP micellar films deposited on electropolished aluminum substrates with improved ordering by solvent annealing, thus transferring the template pores to the aluminum surface. Subsequent anodization in concentrated sulfuric acid enabled the generation of nanochannels with the same center-to-center distance and long-range ordering as the BCP template. This method overcomes the limitations of conventional lithography, making it possible to produce porous aluminum oxides with smaller pore sizes (<50 nm) and long-range ordering.[67] Furthermore, to obtain deeper pores, there should be an adequate etch contrast between the substrate that is to be etched and the etching mask. To this end, Park et al. evaporated an additional thin layer of gold onto the surface of a nanoporous PS-*b*-P4VP film supported on a silicon substrate at a glancing angle to prevent gold deposition on the pore walls. They obtained highly ordered nanopores in silicon substrates with a relatively high aspect ratio of ≈3, which was not achievable using the bare BCP mask without the help of the additional layer of gold (**Figure 4**).[68] Moreover, in another work, they demonstrated the versatility by fabricating different modes of surface patterns using this method. They were able to delicately control the location of gold selectively on the surface of the reconstructed PS-*b*-P4VP, in the pore, or both

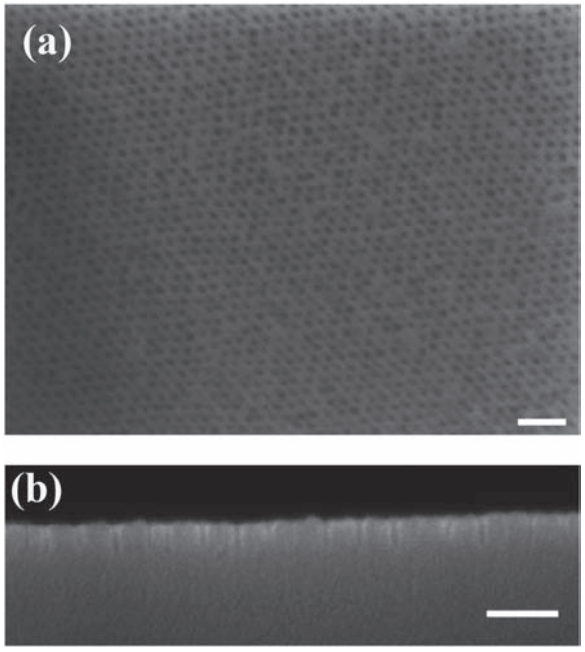

Figure 4. Scanning electron microscopy images of highly ordered arrays of nanopores fabricated on the silicon substrate via reactive ion etching through an etching mask of a gold-coated, reconstructed PS-*b*-P4VP film: a) top view and b) cross-sectional view. A thin layer of gold was evaporated on the surface of the BCP film to enhance the etching contrast with silicon. The scale bar represents 100 nm. Adapted with permission.[68] Copyright 2008, American Chemical Society.

by gold evaporation through a glancing angle. They obtained three different gold masks or templates that could be used in pattern transfer onto silicon substrates.[48]

This chemical heterogeneity of the blocks was also used for surface patterning. Hwang and co-workers fabricated a micropatterned hydrophilic/hydrophobic surface by selectively opening micelles in local regions on PS-*b*-P4VP films using poly(dimethylsiloxane) (PDMS) channels where the ethanol vapor was filled and confined to expose the covered underlying micellar film. The opened areas were relatively hydrophilic because P4VP chains were exposed to the free surface, while the areas that were in direct contact with the PDMS were hydrophobic because they were protected from exposure to ethanol and retained their initial PS chains on the surface. This contrast in the hydrophilicity of the exposed and unexposed regions was demonstrated by moisture adsorption during which water vapor condensed, forming droplets selectively on the hydrophilic exposed regions,[69] as shown in **Figure 5**. Similarly, Meister et al. showed the local micelle opening on PS-*b*-P2VP micellar films for the preparation of a micropatterned surface with a controllable arrangement of nanoscale protrusions (pristine micelles) and concaves (opened micelles). They delivered attoliter amounts of glycerol, a selective solvent for P2VP domains, with a high lateral accuracy to select areas of micellar films using a specially designed AFM cantilever as the nanodispenser. Micelles in areas in contact with the deposited glycerol were opened through the confined swelling mechanism, while the untouched regions retained the initial morphology of

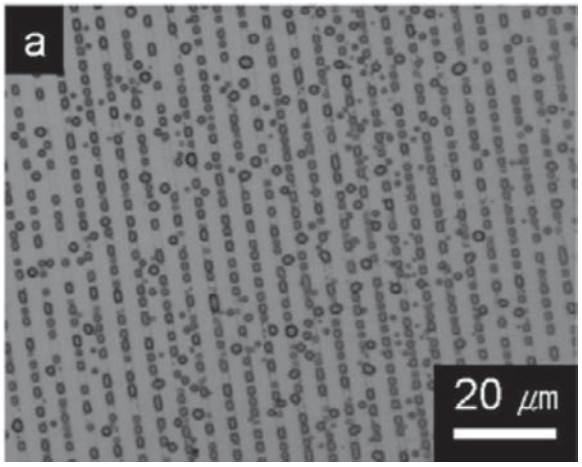

Figure 5. The optical microscopy image of water moisture adsorption on the surface of a PS-*b*-P4VP micellar film with alternating stripes (width = 2 μm, periodicity = 4 μm) of open and closed micelles. The micelles were opened by exposing select regions of the BCP film to ethanol vapor. Water moisture condensed predominantly on the ethanol-exposed regions because of their high hydrophicility caused by the P4VP chains migrating to the surface. Reproduced with permission.[69] Copyright 2005, Institute of Physics.

pristine micelle. The shape and size of the opened area could be tuned by varying the movement mode and trace of the AFM cantilever (**Figure 6**).[70] In contrast to the local micelle opening at selective positions previously described, Park et al. selectively passivated some areas of PS-*b*-P4VP films by crosslinking both the PS and P4VP domains using electron beam (e-beam) lithography and found that the P4VP components in the regions exposed to the e-beam lost their ability to swell in polar solvents. They then treated the BCP film with ethanol and surface reconstruction occurred only in areas that were not exposed to the e-beam, producing a structural contrast between micelle protrusions on the e-beam crosslinked areas and the pores on the rest of the film. Ni was evaporated on the template that was subjected to e-beam crosslinking and ethanol immersion treatment. They obtained patterned arrays of Ni nanodots with separation distances and sizes similar to the template pores after a lift-off process.[71] E-beam lithography, which is a well-developed technique in nanofabrication, offers the possibility

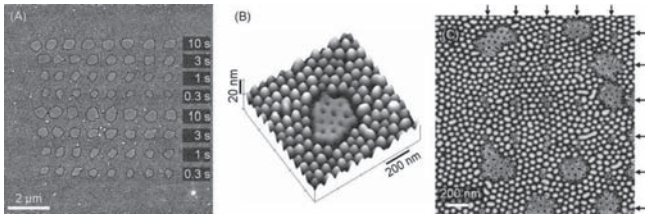

Figure 6. Atomic force microscopy images of PS-*b*-P2VP micellar films with micelles on some areas opened by glycerol droplets locally dispersed by an AFM cantilever. A) Array of spots made of opened micelles after exposure to glycerol droplets. The contact times of the AFM cantilever for each line are noted on the left-hand side. B) Detail of one of the smaller spots. C) Some well-recognizable individual opened micelles. Reproduced with permission.[70] Copyright 2006, Elsevier.

to write arbitrary patterns onto BCP films by crosslinking and consequently affords the freedom to fabricate different materials with the corresponding patterning.

3.3. Guidance of Areal Arrangements of Nanomaterials and Biomolecules

In applications that use the reconstructed amphiphilic BCP films to guide the arrangement of nanoparticles or biomolecules, both the structural variety and chemical heterogeneity of the films have an effect. The pores allow spatial confinement of the species while the polyelectrolyte chains that have migrated on the surface provide the attraction to anchor these species through intermolecular interactions. Sohn et al. first demonstrated the concept of tuning the location of nanoparticles using this swelling-induced morphology reconstruction mechanism (core–corona inversion). Silver precursors loaded into PS-*b*-P4VP micelle cores were displaced to the corona position with the migration of P4VP chains in the reconstruction process, and they were converted to metallic silver nanoparticles under the irradiation of transmission electron microscopy.[33] In contrast, Cho and co-workers utilized the recovering process, in which the P4VP chains withdrew to the initial positions of the P4VP domains in the as-cast micellar films, to prepare arrays of metal nanodots. They spin-coated solutions of metal precursors on the surface of reconstructed PS-*b*-P4VP films on which the P4VP was exposed and had a strong attraction with metal precursors. In the following thermal annealing at a temperature higher than the glass transition temperatures (T_gs) of both blocks, the P4VP chains with the metal precursors recovered to their initial positions, with metal precursors concentrated in these positions. Subsequent oxygen plasma treatment removed the polymer template and converted the metal precursors to arrays of metal nanodots with the periodicity of the parent BCP film.[40a] In a more straightforward method for the fabrication of patterns of nanomaterials, presynthesized nanomaterials were deposited directly onto reconstructed BCP films. The nanomaterials were predominantly deposited into the porous regions because of capillary force when the two constituent blocks were neutral to the nanomaterials. Intermolecular attraction made an additional, and sometimes dominant, contribution when the nanomaterial had selectivity to one block. For example, Son and co-workers fabricated PS-*b*-PMMA templates with pores or grooves corresponding to the initial cylindrical or lamellar morphology in PS or PMMA domains by exposing the as-cast films to PS- or PMMA-selective solvents. They demonstrated that different types of nanomaterials, including CdSe@ZnD quantum dots, γ-Fe_2O_3 nanoparticles, and ZnO nanorods, could be exclusively deposited into the concave regions, either pores or grooves, driven only by a capillary force filling during the spin-coating process.[54] However, if amphiphilic BCPs are used, polyelectrolyte-natured blocks exert an additional attraction on the nanomaterials that is typically stronger than the capillary force, thus enhancing the selectivity of the nanomaterials deposited in the concaved domains of the polar blocks. As an example, Gowd et al. deposited citrate-stabilized palladium nanoparticles selectively into the pores or grooves of ethanol-treated PS-*b*-P4VP films with the P4VP cylinders oriented perpendicular or parallel to the substrates in the as-cast films. In this case, both the attraction of the palladium nanoparticles to the P4VP chains and the capillary force played a role, although the latter was minor. Subsequent UV stabilization of the BCP templates and pyrolysis in air led to arrays of palladium nanoparticles or nanowires with periodicity corresponding to that of the parent BCP templates.[72] Guiding the lateral arrangement of biomolecules, such as proteins, DNAs, peptides, etc., is a very interesting and important applications for BCP thin films with both structural variety and chemical heterogeneity. Kumar et al. deposited three different model proteins selectively onto the PS regions of the swelling-induced reconstructed PS-*b*-P4VP films due to the hydrophobic attraction and obtained large-area, high density, and surface-bound protein arrays with tunable repeat spacings. Furthermore, they demonstrated that the protein arrays retained their natural conformation and activity for several months.[73] In addition, protein arrays with tunable periodicity may be fabricated by depositing proteins selectively onto the regions where the polar blocks of amphiphilic BCP are exposed through the conjugated chemistry between proteins and polyelectrolyte-natured polar blocks, for example, polyacrylic acid.[42]

In summary, all the applications discussed in this section share the same advantages, namely, the generated materials inherit the regularity of the parent BCP materials and the structural parameters are easily tuned, with or without the sacrifice of the BCP materials. The regularity and tunability are crucial in their applications. In addition, many more applications are expected in various fields because of the outstanding integrated superiority in pore properties, surface activity, and the preparation convenience of porous BCP films generated using the swelling-induced method.

4. Confined Swelling-Induced Pore Generation in 1D BCP Structures

Swelling-induced pore generation was first discovered in the thin-film configuration of BCP materials. The pore morphology tunability and application diversity of the nanoporous films thus produced were convincingly demonstrated in various thin film systems by different research groups. In addition to 2D thin films, it would be interesting and practically useful to extend this pore-forming mechanism to BCP materials with other configurations and geometries, for example, 1D nanostructures (nanofibers and nanotubes) and 3D bulk materials. In this section, efforts toward the fabrication of 1D porous nanofibers and nanotubes using this method are discussed. Chen et al. reported the first work in the preparation of porous BCP 1D nanostructures using this method. They infiltrated the cylindrical pores of a porous alumina template with a dilute solution of PS-*b*-PEO and obtained hollow nanotubes with diameters of several hundreds of nanometers. In these nanotubes, PEO domains were distributed in a PS matrix as cylinders perpendicular to the wall surface. They released BCP tubes from the templates and exposed them to a 4:1 water:methanol mixture for 24 h to swell the PEO domains, leading to the production of BCP nanotubes with porous walls.[74] Although the final products were 1D nanotubes, the tube wall was very

thin (≈20 nm), comparable to that of a BCP micellar film, and the tubes can be regarded as rolled films with merged ends. Thus, this case of porous nanotubes should be included in the swelling-induced pore generation in BCP thin-film systems section presented previously. The process for swelling-induced morphology reconstruction of solid BCP nanofibers should be different than that for hollow BCP nanotubes, and qualitatively different porous structures are expected because the distribution and arrangement of both the swellable and nonswollen domains change significantly for BCPs in the geometry of solid fibers and hollow tubes. Consequently, there is a large difference between the degrees of confinement of the swellable domains by the nonswollen phases. Furthermore, the complete diffusion of the swelling solvent into thicker BCP nanofibers (diameter typically >100 nm) requires more time than diffusion into BCP thin films, which further slows the reconstruction process for BCP nanofibers. We investigated the morphology reconstruction of BCP nanofibers induced by selective solvent swelling. Solid nanofibers of PS-*b*-P2VP were prepared by infiltrating BCP melts into the porous alumina template, followed by template removal to release the fibers. No obvious porous structure was found if the nanofibers were immersed in ethanol at room temperature, even for months, which is long enough for the PS-*b*-P2VP micellar films to experience adequate morphology reconstruction.[55,75,76] However, pore formation was triggered by elevating the ethanol immersion temperature, for example to 60 °C. The P2VP domains in the released PS-*b*-P2VP nanofibers, which had diameters several times larger than the equilibrium bulk period because of the surface-induced ordering in the high temperature infiltration and annealing process, took the morphology of long cylinders running along the fiber axis embedded in the PS matrix (**Figure 7**a). After 10 min exposure to ethanol at 60 °C, hollow channels appeared at the position of the initial P2VP cylinders and the surface of the cylinders was covered by a thin layer of P2VP chains. The channels retained the orientation of the initial P2VP cylinders and the 1D geometry of the fibers was unchanged (Figure 7a'). It was necessary to elevate the temperature to facilitate the swelling-induced reconstruction of BCP nanofibers because the P2VP domains were almost completely surrounded by thick (>20 nm) PS layers. Consequently, the swelling in the direction perpendicular to the fiber axis was greatly suppressed. The elevated temperature enhanced the degree of swelling in the P2VP domains in ethanol and the segmental mobility of the PS chains. The volume of the P2VP domains expanded by the swelling P2VP chains squeezed the PS surroundings, resulting in the formation of pores along the entire length of the fiber after the P2VP chains collapsed on the pore wall after ethanol evaporation. There is a strong temperature effect on the morphology reconstruction of PS-*b*-P2VP nanofibers, with the general rule that a higher temperature leads to a faster reconstruction because the relaxation processes underlying chain displacement are thermally activated. Thus the corresponding relaxation times should decrease as the temperature increases. The temperature-enhanced morphology reconstruction was also carried out on BCP nanotubes. Chen et al. subjected PS-*b*-P4VP nanotubes to ethylene glycol at a temperature higher than the T_g of the PS matrix and obtained multiple mesoporous 1D nanostructures.[77]

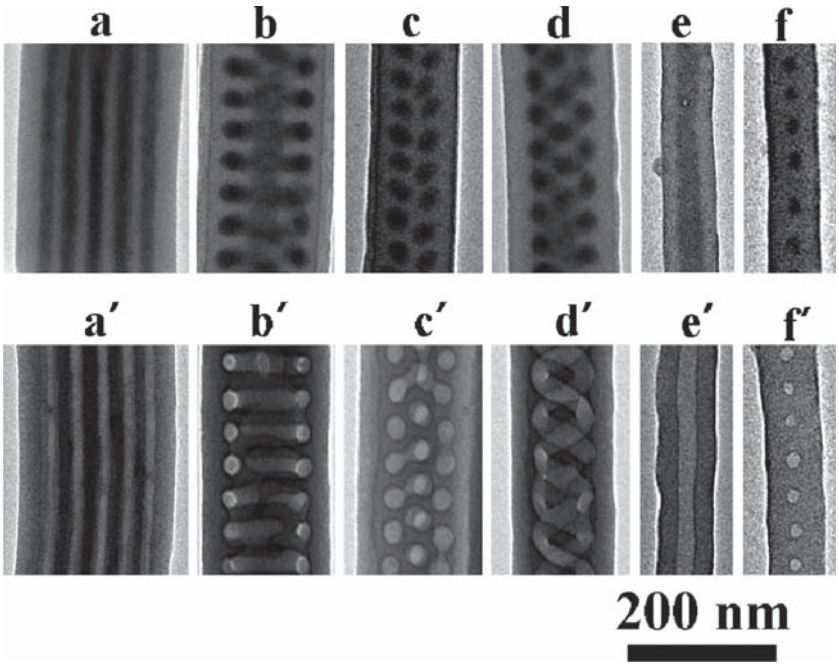

Figure 7. Transmission electron microscopy images of PS-*b*-P2VP nanofibers with different diameters before (a–f) and after (a′–f″) being immersed in ethanol at 60 °C for 10 min. With the change of the template pore diameter, the degree of confinement of BCP inside the pores varies, leading to different morphologies of P2VP domains inside the PS matrix. After ethanol treatment, the P2VP domains cavitate while the profile of P2VP domains remains unchanged. In (a–f), the P2VP domains were selectively stained with iodine vapor to enhance the contrast with the PS matrix during transmission electron microscopy observations.

Furthermore, during the procession of the swelling-induced morphology reconstruction of BCP nanofibers, various intermediate reconstructed morphologies could be observed until isolated spheres formed (micelles with P2VP as the corona and PS as the core). The intermediates included bunches of interconnected strands and strings of spheres, and the reconstruction path may be understood as the transition from the equilibrium morphology of the molten BCP in cylindrical confinement to that of the BCP dissolved in the swelling solvent.[75] One may argue that pores formed in BCP nanofibers during the swelling process may result from the BCP dissolution via a micellization mechanism. However, a high temperature, close to the T_g of the nonswelling component, is necessary to initiate micellization of the solid-state BCP immersed in a selective solvent. During swelling-induced pore generation, the swelling solvent is only heated moderately and the chains of the nonswelling blocks are still in the glassy rigid state; they do not have the flexibility required to bend and collapse into a core of a micelle. In addition, the argument for pore formation through

the micellization dissolution mechanism is not consistent with our experimental observations. First, as shown in Figure 7, the pores were uniform in size and were periodically distributed inside the entire BCP nanofibers. For the BCP dissolution via micellization, pores should at first form randomly on the surface of the BCP nanofibers because the swelling solvent is at first in contact with BCP surface, not the BCP interior, and there are no preferred places on the BCP to form micelles. Second, we could not detect any micelle-like objects in the swelling solvent when pores were already observed in PS-*b*-P2VP nanofibers. Third, during the treatment with a selective solvent, there is an increase in the thickness of the BCP films with a long immersion time. If the pore formation is due to the depletion of BCP chains from BCP materials via micellization, there should be a decrease, or at least no change in thickness, which is in opposition to the significant increase in thickness that is observed experimentally. Therefore, we can exclude the possibility of pore formation during the treatment of BCPs with a selective solvent through the mechanism of BCP dissolution via micellization.

Similar to the swelling of BCP thin films, the reconstruction process of BCP nanofibers was also strongly influenced by the properties of the swelling solvent. For instance, acidic solvents significantly accelerate the reconstruction by protonating pyridine groups. When porous alumina templates with different pore sizes are used, confined P2VP morphologies in the PS matrix, including multiple helices, stacked discs, etc., form according to different degrees of incommensuration and the curvature effect imposed by the small template pores.[78–80] The swelling-induced pore generation mechanism can be applied to these BCP nanofibers with different confined morphologies, and this converts the P2VP domains to pores with regular confined morphologies (Figure 7).[76] On the other hand, the rich variety of pore morphologies also confirms the generality of the swelling-induced pore generation method. Applications of the reconstructed BCP nanofibers and nanotubes also originate from the structural variety and surface activity of the porous structures produced. The easy access to 1D nanostructures with a rich variety of pore morphologies offers a reliable platform for the fabrication of functional inorganic materials with corresponding regular pore morphologies by templating the reconstructed BCP nanofibers and nanotubes with atomic layer deposition or a sol-gel method, followed by template removal.[76,77] In addition, since the polar polyelectrolyte-natured chains are exposed to the pore walls after reconstruction and the reconstruction of the BCP nanofibers and nanotubes is partially reversible, they can be used to guide the decoration and distribution of metal nanoparticles on the surface of porous 1D nanostructures, which may find applications in sensing or microfluidic systems.[81]

5. Swelling-Induced Pore Generation in BCP Bulk Materials

Most efforts in swelling-induced reconstruction have concentrated on BCP materials with at least one nanoscale dimension, such as the 2D BCP thin films and 1D BCP nanofibers and nanotubes discussed above. However, it should be noted that this pore-forming mechanism reaches beyond the nanoscale. It also has great potential for the preparation of porous bulk materials, which are extensively used both in daily life and in many industrial processes. We demonstrated the power of this method for the preparation of BCP-based porous bulk materials.[82] PS-*b*-P2VP thick films, prepared by solution-casting or pellet-melting, with a thickness of up to tens of micrometers were immersed in hot ethanol for hours. Porous films were obtained after the films were withdrawn the films from the ethanol bath and the ethanol evaporated. Identical to the swelling of BCP 1D and 2D systems, the swelling-induced morphology reconstruction of BCP bulk materials also involves a plastic deformation of the glassy PS scaffold to dissipate the stress caused by the osmotic pressure of the solvent inside BCP materials. If cylinder-forming BCP is used, films with bicontinuous porosity can be generated under suitable swelling conditions (**Figure 8**). During swelling, the neighboring, initially isolated P2VP domains grow and fuse with each other due to swelling-induced volume expansion, thus forming another continuous phase that penetrates the PS matrix. With solvent loss during the subsequent drying, the swelling P2VP chains shrink and collapse, while the expanded volume of initial P2VP domains is fixated by the glassy PS, which leads to the formation of pores along the continuous P2VP phase. For very thick BCP films, there may be diffusion-controlled kinetics in the swelling-induced morphology reconstruction. However, this can be avoided or significantly reduced by a two-step swelling process. BCP materials can be first immersed in the solvent at a lower temperature for a longer time, allowing swellable domains to take up a sufficient amount of solvent under a moderate degree of swelling. Subsequently, the swelling temperature can be increased to achieve an adequate degree of swelling, which triggers pore formation.

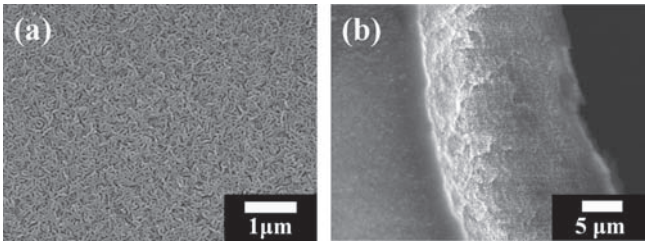

Figure 8. Scanning electron microscopy images of a PS-*b*-P2VP bulk film with a thickness of tens of micrometers immersed in ethanol at 60 °C for 15 h. It has interconnected nanopores throughout the entire film: a) top surface and b) cross section.

The swelling-induced morphology reconstruction of BCP bulk films is also a proceeding transition approaching the final equilibrium state of micelles dissolved in the swelling solvent after long-time (usually days) solvent exposure. Many intermediate reconstructed morphologies with different pore topographies can be frozen and collected via solvent evaporation. These pores are well-defined, with sizes in the range of several tens of nanometers, and can be tuned by changing the swelling conditions, e.g., swelling time, temperature, or using BCPs with different molecular composition. One of the main features of the obtained porous materials is that

the pore walls are covered by P2VP chains, which migrate to the surface during the swelling process. The presence of P2VP chains not only enhances the hydrophilicity of the pore surface but also allows further functionalization of the pores based on the strong activity of the polyelectrolyte-natured P2VP chains. We demonstrated the application of these BCP nanoporous films as templates to prepare metal membranes with reverse pore morphology via electrodeposition and the subsequent removal of BCP templates by solvent dissolution, showing that the BCP materials are recyclable. In addition, we expect good liquid filtration performance of these nanoporous BCP membranes because of their uniform, nanoscale, interconnected pore systems combined with their hydrophilic pore walls covered by P2VP chains, which display a stimuli-responsive property.

This method of swelling-induced pore generation is somewhat similar to the conventional polymer foaming to produce porous materials, which is also a physical process and involves the uptake and release of a foreign agent (gas in the case of foaming, liquid or vapor of solvent in the case of BCP swelling) by the polymer. However, conventional polymer foaming is typically carried out at a temperature close to or higher than the T_g of the polymer material. The dissolution of foreign agents in a polymer is non-selective, and pores can nucleate randomly in the polymer, anywhere other than the area near the polymer surface, because of the fast escape of the gas. As a result polymer foaming typically produces large pores, usually with micrometer or tens of micrometers dimensions, with a wide distribution of pore sizes, and, even worse, with a dense skin layer preventing the access of the inner pores by the ambient.[83,84] The pore properties of the foaming materials are in stark contrast to those of the swelling-induced BCP porous materials, which have nanoscale, uniform, and open pore systems. In an earlier work by Yokoyama and coworkers, compressed carbon dioxide was used to selectively swell the fluorinated domains of BCP materials and obtain cellular monoliths with closed and isolated nanopores embedded in nonporous surface skin.[85] This work can be considered to be an early instance of swelling-induced pore generation in BCP bulk materials. However, the swelling degree of the fluorinated blocks was severely limited because of the poor solubility of carbon dioxide compared to conventional liquid solvents. Consequently, pores nucleating separately remained isolated, with no chance to merge, and they could not break the wrapping of the nonswollen blocks. However, with the aid of supercritical fluids, the uptake of liquid solvents by thick BCP materials will be strongly enhanced due to the gas-like diffusion property of supercritical fluids, facilitating the swelling of thick BCP materials with no need to increase the temperature. The significance of this swelling-induced pore-making method for producing porous bulk materials lies in the synergy of the distinct advantages of this method. First, the production process, composed of dipping in solvent and drying in air, is extremely simple. Second, there is no weight loss in BCP materials, which is important because weight loss may weaken the mechanical stability of the materials and lead to by-products that are left in the solvent, thus preventing direct reuse. Third, this swelling-induced pore generation process is reversible. The pores can be partially or completely recovered, offering the possibility to use the porous materials in intelligent systems where pore opening and closing need to be switched. Fourth, the pore wall is very chemically active, allowing further modifications to the pore surface that render additional functions to the porous materials. Finally, the sub-50-nm pore size and narrow pore size distribution, which are both difficult to obtain via other methods, make it possible to use the porous materials in some advanced applications, such as high-resolution separation.[22c,29,86–89]

6. Concluding Remarks

As an emerging method for the preparation of nanoporous materials, swelling-induced pore generation shows its generality by successfully producing pores in various BCP materials with different dimensions that include 2D thin films, 1D nanofibers and nanotubes, and bulk materials. This also makes the method attractive to researchers outside the nano-community. This strategy has advantages compared to other pore-making methods that include its extreme process simplicity, well-defined pore morphologies with sizes typically <50 nm, pore formation without sacrificing any components of the material, and the surface activity of the pore wall, the recovery of the formed pores. However, it should be noted that this method has its own drawback, which is the relatively low porosity of the resultant porous materials, typically limited to 20–30% because the nonswollen blocks in the starting BCPs must be the major component to hold the infrastructure of the BCP materials in the swelling process and pores can only form in the swellable minority domains (volume ratio <50%) by pushing portions of the swelling blocks out of their initial positions. Further efforts need to be devoted to increasing the porosity of materials produced by this method. In addition, there is a lack of in-depth understanding on the mechanism of the confined swelling-induced pore generation; for example, the boundary conditions for swelling, the subtle interplay between the solvent and the constituent blocks, the conformation changes of both the swelling and nonswollen blocks with the evaporation of solvent, the chain displacement of the nonswollen blocks dragged by the swelling and shrinking of the swelling blocks, etc. still remain largely open. Theoretical endeavors need to put into this area to address these open questions, and to guide how to optimize the swelling process experimentally to achieve improved pore systems through this method. Furthermore, to promote the applications of this method on a larger scale in more diverse fields, attention should be paid to making pores in commercial BCP materials rather than using expensive, laboratory-synthesized amphiphilic BCPs. Systematic work is needed to identify suitable swelling solvents and to define swelling conditions to trigger the pore formation in commercial staple BCPs, such as triblock copolymers of polystyrene and polybutadiene or polyisoprene (SBS and SIS), which are traditionally used as thermal plastics. The constituent blocks of both of these materials are hydrophobic and have close dissolution properties. Nevertheless, it is expected that an increasing range of applications for this method will be seen, as is predetermined by its synergic advantages.

Acknowledgements

This work is financially supported by the National Natural Science Foundation of China (21004033), the Jiangsu Natural Science Foundation (BK2009358), the Open Research Fund of State Key Laboratory of Chemical Resource Engineering (Beijing University of Chemical Technology), Doctoral Program Foundation of Institutions of Higher Education of China (20103221120001), the Scientific Research Foundation for Returned Scholars, Ministry of Education of China, and the Project of Priority Academic Program Development of Jiangsu Higher Education Institutions (PAPD).

Received: October 31, 2010
Revised: February 21, 2011
Published online: April 5, 2011

[1] A. Stein, *Adv. Mater.* **2003**, *15*, 763.
[2] I. Tokarev, S. Minko, *Adv. Mater.* **2010**, *22*, 3446.
[3] C. D. Liang, Z. J. Li, S. Dai, *Angew. Chem. Int. Ed.* **2008**, *47*, 3696.
[4] A. Stein, Z. Y. Wang, M. A. Fierke, *Adv. Mater.* **2009**, *21*, 265.
[5] A. Stein, R. C. Schroden, *Curr. Opin. Solid State Mater. Sci.* **2001**, *5*, 553.
[6] C. C. Striemer, T. R. Gaborski, J. L. McGrath, P. M. Fauchet, *Nature* **2007**, *445*, 749.
[7] G. S. Chai, I. S. Shin, J. S. Yu, *Adv. Mater.* **2004**, *16*, 2057.
[8] S. K. Seshadri, H. M. Alsyouri, Y. S. Lin, *Microporous Mesoporous Mater.* **2010**, *129*, 228.
[9] J. H. Bang, K. S. Suslick, *Adv. Mater.* **2009**, *21*, 3186.
[10] F. S. Bates, G. H. Fredrickson, *Annu. Rev. Phys. Chem.* **1990**, *41*, 525.
[11] I. W. Hamley, *Prog. Polym. Sci.* **2009**, *34*, 1161.
[12] V. Abetz, P. F. W. Simon, *Adv. Polym. Sci.* **2005**, *189*, 125.
[13] N. A. Lynd, A. J. Meuler, M. A. Hillmyer, *Prog. Polym. Sci.* **2008**, *33*, 875.
[14] M. Moffitt, K. Khougaz, A. Eisenberg, *Acc. Chem. Res.* **1996**, *29*, 95.
[15] M. Lazzari, M. A. Lopez-Quintela, *Adv. Mater.* **2003**, *15*, 1583.
[16] R. A. Segalman, *Mater. Sci. Eng., R* **2005**, *48*, 191.
[17] J. Bang, U. Jeong, D. Y. Ryu, T. P. Russell, C. J. Hawker, *Adv. Mater.* **2009**, *21*, 4769.
[18] Y. Wan, H. F. Yang, D. Y. Zhao, *Acc. Chem. Res.* **2006**, *39*, 423.
[19] Y. Wan, D. Y. Zhao, *Chem. Rev.* **2007**, *107*, 2821.
[20] T. Thurn-Albrecht, J. Schotter, C. A. Kastle, N. Emley, T. Shibauchi, L. Krusin-Elbaum, K. Guarini, C. T. Black, M. T. Tuominen, T. P. Russell, *Science* **2000**, *290*, 2126.
[21] Y. Wang, U. Gösele, M. Steinhart, *Chem. Mater.* **2008**, *20*, 379.
[22] a) E. J. W. Crossland, M. Kamperman, M. Nedelcu, C. Ducati, U. Wiesner, D. M. Smilgies, G. E. S. Toombes, M. A. Hillmyer, S. Ludwigs, U. Steiner, H. J. Snaith, *Nano Lett.* **2009**, *9*, 2807; b) E. J. W. Crossland, M. Nedelcu, C. Ducati, S. Ludwigs, M. A. Hillmyer, U. Steiner, H. J. Snaith, *Nano Lett.* **2009**, *9*, 2813; c) L. M. Pitet, M. A. Amendt, M. A. Hillmyer, *J. Am. Chem. Soc.* **2010**, *132*, 8230.
[23] a) Y. T. Tseng, W. H. Tseng, C. H. Lin, R. M. Ho, *Adv. Mater.* **2007**, *19*, 3584; b) H. Y. Hsueh, H. Y. Chen, M. S. She, C. K. Chen, R. M. Ho, S. Gwo, H. Hasegawa, E. L. Thomas, *Nano Lett.* **2010**, *10*, 4994.
[24] a) M. Park, C. Harrison, P. M. Chaikin, R. A. Register, D. H. Adamson, *Science* **1997**, *276*, 1404; b) T. Hashimoto, *Langmuir* **1997**, *13*, 6869.
[25] V. Z. H. Chan, J. Hoffman, V. Y. Lee, H. Iatrou, A. Avgeropoulos, N. Hadjichristidis, R. D. Miller, E. L. Thomas, *Science* **1999**, *286*, 1716.
[26] D. H. Kim, K. H. A. Lau, W. Joo, J. Peng, U. Jeong, C. J. Hawker, J. K. Kim, T. P. Russell, W. Knoll, *J. Appl. Phys. B* **2006**, *110*, 15381.
[27] W. V. Zoelen, G. T. Brinke, *Soft Matter* **2009**, *5*, 1568.
[28] O. Ikkala, G. T. Brinke, *Science* **2002**, *295*, 2407.
[29] S. Y. Yang, I. Ryu, H. Y. Kim, J. K. Kim, S. K. Jang, T. P. Russell, *Adv. Mater.* **2006**, *18*, 709.
[30] M. A. Hillmyer, *Adv. Polym. Sci.* **2005**, *190*, 137.
[31] D. A. Olson, L. Chen, M. A. Hillmyer, *Chem. Mater.* **2008**, *20*, 869.
[32] Y. Boontongkong, R. E. Cohen, *Macromolecules* **2002**, *35*, 3647.
[33] B. H. Sohn, S. I. Yoo, B. W. Seo, S. H. Yun, S. M. Park, *J. Am. Chem. Soc.* **2001**, *123*, 12734.
[34] T. Matsuyama, Y. Kawata, *J. Appl. Phys.* **2007**, *46*, 3882.
[35] C. Xu, X. F. Fu, M. Fryd, S. Xu, *Nano Lett.* **2006**, *6*, 282.
[36] C. Xu, B. B. Wayland, M. Fryd, K. I. Winey, R. J. Composto, *Macromolecules* **2006**, *39*, 6063.
[37] J. C. Zhao, Q. Wang, C. D. Qiao, S. C. Jiang, *Chem. J. Chinese U.* **2005**, *26*, 362.
[38] P. J. Flory, *J. Chem. Phys.* **1950**, *18*, 108.
[39] P. J. Flory, *J. Chem. Phys.* **1949**, *17*, 303.
[40] Z. Q. Chen, C. C. He, F. B. Li, L. Tong, X. Z. Liao, Y. Wang, *Langmuir* **2010**, *26*, 8869.
[41] a) H. Cho, H. Park, T. P. Russell, S. Park, *J. Mater. Chem.* **2010**, *20*, 5047; b) L. Tsarkova, G. J. A. Sevink, G. Krausch, *Adv. Polym. Sci.* **2010**, *227*, 33; c) U. Zettl, A. Knoll, L. Tsarkova, *Langmuir* **2010**, *26*, 6610.
[42] A. C. Miller, R. D. Bennett, P. T. Hammond, D. J. Irvine, R. E. Cohen, *Macromolecules* **2008**, *41*, 1739.
[43] S. Krishnamoorthy, R. Pugin, J. Brugger, H. Heinzelmann, C. Hinderling, *Adv. Funct. Mater.* **2006**, *16*, 1469.
[44] L. Wang, F. Montagne, P. Hoffmann, R. Pugin, *Chem. Commun.* **2009**, *25*, 3798.
[45] R. D. Bennett, A. C. Miller, N. T. Kohen, P. T. Hammond, D. J. Irvine, R. E. Cohen, *Macromolecules* **2005**, *38*, 10728.
[46] S. Park, J. Y. Wang, B. Kim, W. Chen, T. P. Russell, *Macromolecules* **2007**, *40*, 9059.
[47] T. Xu, J. Stevens, J. A. Villa, J. T. Goldbach, K. W. Guarim, C. T. Black, C. J. Hawker, T. R. Russell, *Adv. Funct. Mater.* **2003**, *13*, 698.
[48] S. Park, J. Y. Wang, B. Kim, T. P. Russell, *Nano Lett.* **2008**, *8*, 1667.
[49] S. Krishnamoorthy, R. Pugin, J. Brugger, H. Heinzelmann, A. C. Hoogerwerf, C. Hinderling, *Langmuir* **2006**, *22*, 3450.
[50] X. Li, S. J. Tian, Y. Ping, D. H. Kim, W. Knoll, *Langmuir* **2005**, *21*, 9393.
[51] A. Laforgue, C. G. Bazuin, R. E. Prud'homme, *Macromolecules* **2006**, *39*, 6473.
[52] T. Xu, J. T. Goldbach, M. J. Misner, S. Kim, A. Gibaud, O. Gang, B. Ocko, K. W. Guarini, C. T. Black, C. J. Hawker, T. P. Russell, *Macromolecules* **2004**, *37*, 2972.
[53] K. W. Guarini, C. T. Black, S. H. I. Yeung, *Adv. Mater.* **2002**, *14*, 1290.
[54] J. G. Son, W. K. Bae, H. M. Kang, P. F. Nealey, K. Char, *ACS Nano* **2009**, *3*, 3927.
[55] Y. Wang, L. Tong, M. Steinhart, *ACS Nano* **2011**, *5*, 1928.
[56] L. Li, H. Yokoyama, T. Nemoto, K. Sugiyama, *Adv. Mater.* **2004**, *16*, 1226.
[57] D. L. Tomasko, H. B. Li, D. H. Liu, X. M. Han, M. J. Wingert, L. J. Lee, K. W. Koelling, *Ind. Eng. Chem. Res.* **2003**, *42*, 6431.
[58] T. Kentaro, W. Yusuke, O. Masahiro, *Macromol. Mater. Eng.* **2008**, *293*, 589.
[59] R. Zhang, H. Yokoyama, *Macromolecules* **2009**, *42*, 3559.
[60] H. Masuda, F. Fukuda, *Science* **1995**, *268*, 1466.
[61] M. Wirtz, C. R. Martin, *Adv. Mater.* **2003**, *15*, 455.
[62] Y. Wang, M. Becker, L. Wang, J. Liu, R. Scholz, J. Peng, U. Gösele, S. H. Christiansen, D. H. Kim, M. Steinhart, *Nano Lett.* **2009**, *9*, 2384.
[63] Y. H. Qiao, D. Wang, J. M. Buriak, *Nano Lett.* **2007**, *7*, 464.
[64] Y. Wang, J. Q. Liu, S. Christiansen, D. H. Kim, U. Gösele, M. Steinhart, *Nano Lett.* **2008**, *8*, 3993.

[65] J. Chai, D. Wang, X. N. Fan, J. M. Buriak, *Nat. Nanotechnol.* **2007**, *2*, 500.
[66] J. Chai, J. M. Buriak, *ACS Nano* **2008**, *2*, 489.
[67] B. Y. Kim, S. J. Park, T. J. McCarthy, T. P. Russell, *Small* **2007**, *3*, 1869.
[68] S. Park, J. Y. Wang, B. Kim, J. Xu, T. P. Russell, *ACS Nano* **2008**, *2*, 766.
[69] W. Hwang, M. H. Ham, B. H. Sohn, J. Huh, Y. S. Kang, W. Jeong, J. M. Myoung, C. Park, *Nanotechnology* **2005**, *16*, 2897.
[70] A. Meister, S. Krishnamoorthy, C. Hinderling, R. Pugin, H. Heinzelmann, *Microelectron. Eng.* **2006**, *83*, 1509.
[71] S. Park, O. Yavuzcetin, B. Kim, M. T. Tuominen, T. P. Russell, *Small* **2009**, *5*, 1064.
[72] E. B. Gowd, B. Nandan, M. K. Vyas, N. C. Bigall, A. Eychmuller, H. Schlorb, M. Stamm, *Nanotechnology* **2009**, *20*, 10.
[73] N. Kumar, O. Parajuli, J. I. Hahm, *J. Phys. Chem. B* **2007**, *111*, 4581.
[74] J. T. Chen, M. F. Zhang, L. Yang, M. Collins, J. Parks, A. Avallone, T. P. Russell, *J. Polym. Sci., Part B: Polym. Phys.* **2007**, *45*, 2912.
[75] Y. Wang, U. Gösele, M. Steinhart, *Nano Lett.* **2008**, *8*, 3548.
[76] Y. Wang, Y. Qin, A. Berger, E. Yau, C. C. He, L. B. Zhang, U. Gösele, M. Knez, M. Steinhart, *Adv. Mater.* **2009**, *21*, 2763.
[77] D. Chen, S. Park, J.-T. Chen, E. Redston, T. P. Russell, *ACS Nano* **2009**, *3*, 2827.
[78] K. Shin, H. Q. Xiang, S. I. Moon, T. Kim, T. J. McCarthy, T. P. Russell, *Science* **2004**, *306*, 76.
[79] H. Xiang, K. Shin, T. Kim, S. Moon, T. J. McCarthy, T. P. Russell, *J. Polym. Sci. Part B: Polym Sci* **2005**, *43*, 3377.
[80] B. Yu, P. Sun, T. Chen, Q. Jin, D. Ding, B. Li, *Phys. Rev. Lett.* **2006**, *96*, 138306.
[81] S. Chang, S. Singamaneni, E. Kharlampieva, S. L. Young, V. V. Tsukruk, *Macromolecules* **2009**, *42*, 5781.
[82] Y. Wang, C. C. He, W. H. Xing, F. B. Li, L. Tong, Z. Q. Chen, X. Z. Liao, M. Steinhart, *Adv. Mater.* **2010**, *22*, 2068.
[83] R. J. Pugh, *Adv. Colloid Interf. Sci.* **1996**, *64*, 67.
[84] H. Tanaka, *Adv. Mater.* **2009**, *21*, 1872.
[85] H. Yokoyama, L. Li, T. Nemoto, K. Sugiyama, *Adv. Mater.* **2004**, *16*, 1542.
[86] a) W. A. Phillip, J. Rzayev, M. A. Hillmyer, E. L. Cussler, *J. Membr. Sci.* **2006**, *286*, 144; b) L. Chen, W. A. Phillip, E. L. Cussler, M. A. Hillmyer, *J. Am. Chem. Soc.* **2007**, *129*, 13786; c) W. A. Phillip, M. Amendt, B. O'Neill, L. Chen, M. A. Hillmyer, E. L. Cussler, *ACS Appl. Mater. Interfaces* **2009**, *1*, 472; d) W. A. Phillip, B. O'Neill, M. Rodwogin, M. A. Hillmyer, E. L. Cussler, *ACS Appl. Mater. Interfaces* **2010**, *2*, 847; e) E. A. Jackson, M. A. Hillmyer, *ACS Nano* **2010**, *4*, 3548.
[87] a) K. V. Peinemann, V. Abetz, P. F. W. Simon, *Nat. Mater.* **2007**, *6*, 992; b) S. P. Nunes, R. Sougrat, B. D. H. Anjum, A. R. Behzad, L. Zhao, N. Pradeep, J. Pinnau, I. U. Vainio, U. K. V. Peinemann, *Macromolecules* **2010**, *43*, 8079.
[88] a) S. Y. Yang, J. Park, J. Yoon, M. Ree, S. K. Jang, J. K. Kim, *Adv. Funct. Mater.* **2008**, *18*, 1371; b) S. Y. Yang, J. A. Yang, E. S. Kim, G. Jeon, E. J. Oh, K. Y. Choi, S. K. Hahn, J. K. Kim, *ACS Nano* **2010**, *4*, 3817.
[89] a) R. Pugin, N. Blondiaux, C. T. Popa, P. Niedermann, M. Liley, M. Giazzon, N. Mathey, A. Hubbell, H. Heinzelmann, *J. Photopolym. Sci. Technol.* **2009**, *22*, 223; b) X. F. Li, C. A. Fustin, N. Lefevre, J. F. Gohy, S. De Feyter, J. De Baerdemaeker, W. Egger, I. F. J. Vankelecom, *J. Mater. Chem.* **2010**, *20*, 4333.